

Probing the stability and magnetic properties of magnetosome chains in freeze-dried magnetotactic bacteria

Philipp Bender,^{*,†} Lourdes Marcano,^{‡,¶} Iñaki Orue,[§] Diego Alba Venero,^{||} Dirk
Honecker,[⊥] Luis Fernández Barquín,[#] Alicia Muela,^{@,Δ} and M. Luisa
Fdez-Gubieda^{¶,@}

[†]*Physics and Materials Science Research Unit, University of Luxembourg, 1511
Luxembourg, Grand Duchy of Luxembourg*

[‡]*Helmholtz-Zentrum Berlin für Materialien und Energie, 12489 Berlin, Germany*

[¶]*Dpto. Electricidad y Electrónica, Universidad del País Vasco – UPV/EHU, 48940
Leioa, Spain.*

[§]*SGIker, Universidad del País Vasco – UPV/EHU, 48940 Leioa, Spain*

^{||}*ISIS Neutron and Muon Facility, Rutherford Appleton Laboratory, Chilton, OX11 0QX,
United Kingdom*

[⊥]*Large Scale Structures group, Institut Laue-Langevin, 38042 Grenoble, France*

[#]*CITIMAC, Universidad de Cantabria, 39005 Santander, Spain*

[@]*BCMaterials, Basque Center for Materials, Applications and Nanostructures, UPV/EHU
Science Park, 48940 Leioa, Spain*

^Δ*Dpto. Immunología, Microbiología y Parasitología, Universidad del País Vasco – UPV/EHU,
48940 Leioa, Spain.*

E-mail: philipp.bender@uni.lu

Abstract

Magnetospirillum gryphiswaldense contain typically 15-30 magnetite nanoparticles, i.e. magnetosomes, with diameters of around 40 nm. They are arranged in linear chains inside the bacteria, which makes them a paradigm of 1D magnetic nanostructures. Here we perform magnetometry and polarized small-angle neutron scattering experiments on a powder of freeze-dried *M. gryphiswaldense*. We confirm that the magnetosomes are single-domain particles with uniaxial anisotropy and that an alignment of the particle moments in field direction occurs exclusively by a Néel-like rotation. We can show that the chain structure is preserved also after application of large magnetic fields of up to 1 T and that dipolar interactions, which play a vital role during the chain formation, are in fact negligible regarding the magnetization behavior of the 1D magnetosome chains.

Keywords

magnetotactica bacteria, magnetosomes, dipolar interactions, mechanical stability, first-order reversal curves, small-angle neutron scattering

Magnetotactic bacteria are a microorganism able to align and navigate along geomagnetic fields thanks to the presence of chains of magnetic nanoparticles, called magnetosomes.^{1,2} In particular, *Magnetospirillum gryphiswaldense* synthesize high-purity magnetite cores with cubo-octahedral shape and a mean diameter of around 40 nm, with a narrow size distribution.³ A previous study has shown that the particles are arranged in slightly bent, helical-shaped chains due to a competition between dipolar interactions and elastic forces during the chain formation.⁴ This natural magnetic arrangement can be considered a paradigm of 1D magnetic nanoarchitecture.

In general, linear assemblies of magnetic nanoparticles have received considerable interest in various fields including micromechanical sensors,^{5,6} microfluidics,⁷ micro-swimmers⁸ and also fundamental science.⁹ Different techniques exist to synthesize 1D nanoparticle chains¹⁰⁻¹² however, thanks to the high biological control imposed in the synthesis of the

magnetosomes, magnetotactic bacteria produce 1D nanostructures with high reproducibility and quality.¹³ Due to their exceptional properties *M. gryphiswaldense* remain highly investigated, motivating several experimental studies where their magnetic properties were evaluated.^{4,13-15} In¹⁶ and¹⁷ however, it was observed that already small fields (i.e. small magnetic torques) of around 30 mT can be sufficient to break-up the particle chains within alive bacteria while dispersed in colloidal suspension.

In this work we probe the response of freeze-dried *M. gryphiswaldense* to magnetic fields, which may have different elastic properties compared to the swollen bacteria in suspension. We use a combination of DC magnetometry and small-angle neutron scattering (SANS) to investigate a powder of randomly oriented, freeze-dried bacteria. Due to the surrounding organic mass, interactions between neighboring chains can be neglected, enabling us to exclusively study the individual 1D particle chains. From the polarized SANS results we can deduce information about the magnetic structure of the particles and gain additionally insight into the nanostructure of the 1D chains, enabling us to test their mechanical stability in high fields, i.e. high magnetic torques. By analyzing Henkel and first-order reversal curves (FORC) of the bacteria powder we then evaluate the amount of inter-particle interactions between the particles within the 1D chains.

M. gryphiswaldense strain MSR-1 (DMSZ 6631) was grown in a flask standard medium (FSM).¹⁸ The culture was carried out in three-fourths full bottles at 28 °C, without agitation. After 120 h, when the magnetosomes were well-formed,³ the bacteria cells were collected and fixed in 2% glutaraldehyde. Finally, after repeated washings with distilled water, the bacteria were freeze-dried, resulting in a powder sample with random orientation of the particle chains, i.e. a structurally and magnetically isotropic sample. Additionally, we grew and freeze-dried bacteria without magnetosomes³, which were measured by SANS as a background sample to subtract from the magnetotactic bacteria signal.

To characterize the bacteria, we first performed transmission electron microscopy (TEM, JEOL JEM-1400Plus) on unstained bacteria adsorbed onto carbon-coated copper grids, and

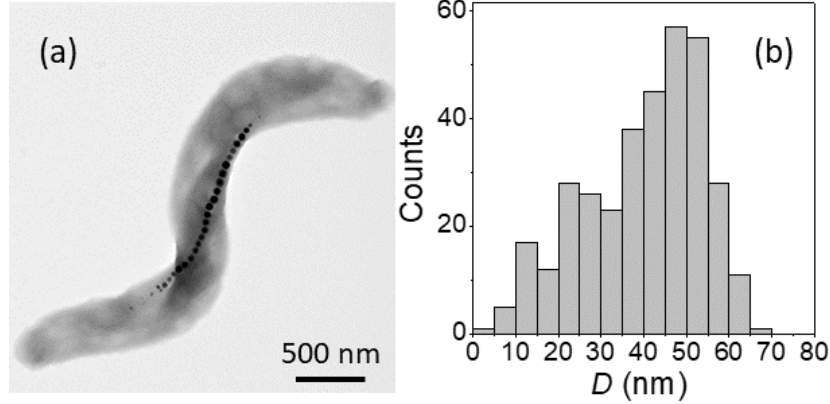


Figure 1: (a) TEM image of a *M. gryphiswaldense* with a chain of around 30 magnetosomes, and (b) the size-distribution of the magnetosomes ($N = 347$).

used ImageJ¹⁹ for the image processing and analysis. Fig. 1(a) shows a typical TEM image of a *M. gryphiswaldense* containing a chain of magnetosomes. The observed chain is composed of uniformly sized magnetosomes except for those at both ends of the chain, which are slightly smaller.⁴ This results in a broadening of the size histogram (Fig. 1(b)), whose mean value amounts to $\langle D \rangle = 40$ nm. Typically, the number of magnetosomes per cell is around 15 to 30, with a center-to-center distance between neighboring particles of about 60 nm.⁴ Additionally, it can be noted that due to the surrounding organic matrix the individual 1D chains are separated from each other, meaning that interactions between neighboring chains can be neglected, and that we can study the magnetization behaviour of the individual chains.

The SANS experiment of the bacteria powder sample was conducted at room temperature with the Larmor instrument at ISIS neutron and muon source, Rutherford Appleton Laboratory, where we performed polarized SANS (SANSPOL, incoming neutrons are polarized spin-up or spin-down). The magnetic field \mathbf{H} was applied perpendicular to the incoming neutron beam ($\mathbf{k} \parallel \mathbf{e}_x \perp \mathbf{H} \parallel \mathbf{e}_z$). The resulting SANS cross-sections can be written in case of

an isotropic magnetization distribution in \widetilde{M}_y as²⁰

$$I^\pm(\mathbf{q}) \propto |\widetilde{N}|^2 + b_h^2 \left(|\widetilde{M}_x|^2 + |\widetilde{M}_y|^2 \cos^2 \Theta + |\widetilde{M}_z|^2 \sin^2 \Theta \right) \mp b_h (\widetilde{N} \widetilde{M}_z^* + \widetilde{N}^* \widetilde{M}_z) \sin^2 \Theta, \quad (1)$$

where the index $+/-$ indicates the polarization of the incoming beam, i.e. spin-up or spin-down. Here Θ is the angle between the scattering vector $\mathbf{q} = (0, q_y, q_z)$ and the magnetic field \mathbf{H} , and $b_h = 2.7 \cdot 10^{-15} \text{ m}/\mu_B$, where μ_B is the Bohr magneton. Moreover, $\widetilde{N}(\mathbf{q})$ and $\widetilde{M}_{x,y,z}(\mathbf{q})$ denote the Fourier transforms of the nuclear scattering length density and of the magnetization in the x -, y - and z -directions, respectively. From the measured SANS POL intensities, the nuclear-magnetic cross-terms $I_{\text{cross}}(q) \propto (\widetilde{N} \widetilde{M}_z^* + \widetilde{N}^* \widetilde{M}_z)$ can be determined as a function of the applied field from the sector perpendicular to \mathbf{H} of the residual scattering pattern $I^-(\mathbf{q}) - I^+(\mathbf{q}) = I_{\text{cross}}(q) \sin^2 \Theta$. Analysis of this cross-term is in particular useful for systems where the nuclear scattering dominates the magnetic scattering, which is usually the case e.g. for iron oxide nanoparticles.^{21,22} We can assume that the nuclear scattering cross-section \widetilde{N} of the bacteria is dominated by the magnetosomes. Thus, in case of a homogeneous magnetization, i.e. single-domain particles with $\widetilde{N} \propto \widetilde{M}_z$, we can write at first approximation for the cross-term $I_{\text{cross}}(q) \propto F^2(q)$, where $F^2(q)$ is the particle form factor, for which we will use here the spherical one.²³ Furthermore, we measured the SANS signal of the empty bacteria as background measurement and subtracted it from the SANS POL intensities $I^\pm(\mathbf{q})$ to be able to determine the nuclear scattering of the magnetosome chains.

Fig. 2 shows the 2D pattern of the residual SANS cross-section $I^-(\mathbf{q}) - I^+(\mathbf{q}) = I_{\text{cross}}(q) \sin^2 \Theta$ at an applied field of 1 T. By azimuthally integrating the intensity in the sector perpendicular to \mathbf{H} ($\Theta = 90^\circ$, $\Delta\Theta = 10^\circ$), we derived the 1D nuclear-magnetic cross-term $I_{\text{cross}}(q)$. In Fig. 3(a), we plot $I_{\text{cross}}(q)$ detected at the maximum field of 1 T and detected at zero field in the demagnetized state and the remanent state, respectively. As can be seen, for the demagnetized state $I_{\text{cross}}(q) \approx 0$ over the whole q -range, which is expected because the

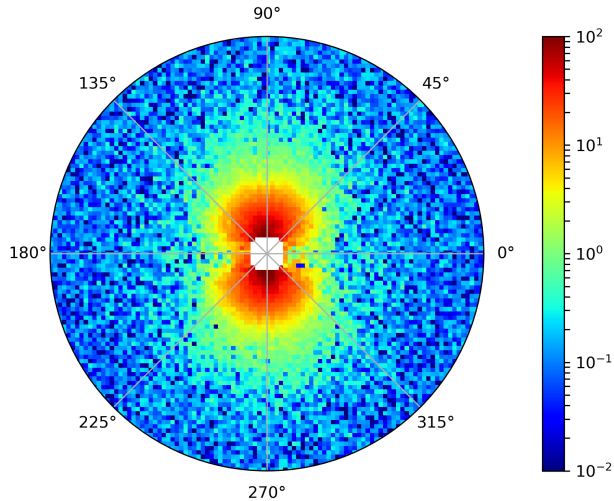


Figure 2: Residual SANSPOLE pattern $I^-(\mathbf{q}) - I^+(\mathbf{q}) = I_{cross}(q)\sin^2\Theta$ in arbitrary units detected at a field strength of $\mu_0 H = 1$ T ($q = 0.045 - 0.5$ nm $^{-1}$). The field \mathbf{H} was applied in horizontal direction along $\Theta = 0^\circ$.

cross-term is directly proportional to the sample magnetization in field direction. In the saturated and the remanent state, on the other hand, we detect finite values, whereby the absolute values of the remanent state are by a factor of 2 smaller than in saturation. This implies a reduced remanence of $m_R/m_S = 0.5$ (here m_R is the remanent moment and m_S the measured moment in saturation), which is the expected value for an isotropic ensemble of single-domain particles with uniaxial anisotropy (i.e. Stoner-Wohlfarth particles).²⁴

From $I_{cross}(q)$ we can additionally estimate the size of the magnetosomes by fitting the 1D cross-sections with the spherical form factor (Fig.3(b)). Assuming a lognormal size distribution, we obtain a mean particle diameter of 35(6) nm (breadth $\sigma = 0.26(9)$), which is in quite a good agreement with the mean particle size according to TEM (Fig. 1), although a little bit smaller. The good agreement between the functional form of the cross-term detected at saturation and remanence (Fig.3(b)) shows, that qualitatively the magnetic cross-section is not altered by applying a magnetic field. This confirms that the particles are in fact (at least at first approximation) single-domain particles and that a rotation of the particle moments in field direction occurs by an internal, homogeneous (i.e. coherent), Néel-like rotation of the atomic magnetic moments inside the individual particles.

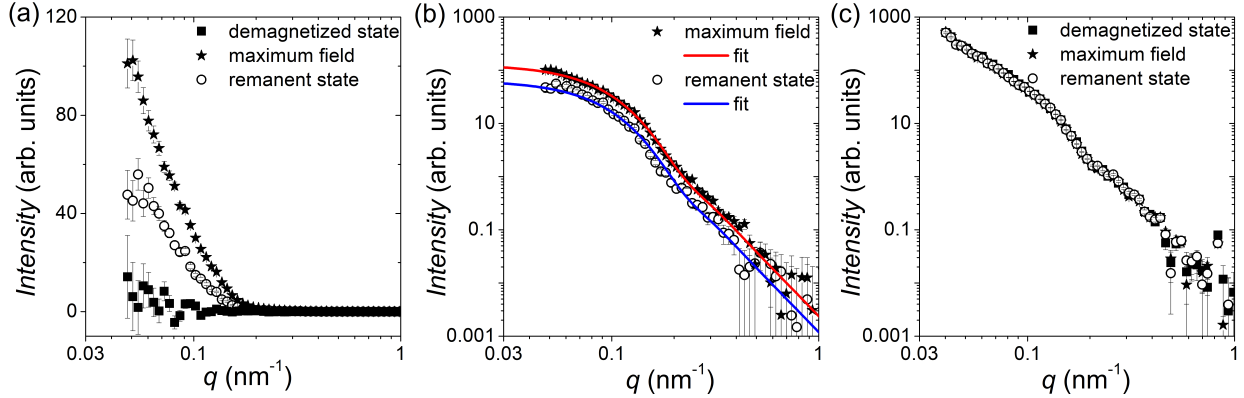


Figure 3: (a) Nuclear-magnetic cross-term $I_{\text{cross}}(q)$ detected at maximum field (i.e. magnetic saturation) and at zero field in the demagnetized state and remanent state, respectively (linear y -scale). (b) Fit of $I_{\text{cross}}(q)$ in the saturated and remanent state with the spherical particle form factor (logarithmic y -scale). (c) Cross-section of $I^+(\mathbf{q})$ parallel to \mathbf{H} in the saturated, demagnetized and remanent state. The scattering intensity of the bacteria without magnetosomes is subtracted.

Fig. 3(c) shows additionally the 1D cross-sections $I(q)$, which we determined by an azimuthal integration of $I^+(\mathbf{q})$ in the sector parallel to \mathbf{H} ($\Theta = 0^\circ$, $\Delta\Theta = 10^\circ$). The scattering intensity of the bacteria without magnetosomes is subtracted such that we can assume that the SANS signal is dominated by the purely nuclear cross-section of the magnetosome chains. We observe that $I(q)$ does not vary with field leading to a perfect overlap of the scattering curves, which shows that $I(q)$ is dominated by the nuclear scattering, and which in turn verifies that the nuclear cross-section is not changed by applying the magnetic fields. Hence we can conclude that the particle chains within the freeze-dried bacteria remain intact and do not rotate, because otherwise we would expect a significant variation between the field-dependent cross-sections. Moreover, the arrangement and separation of the particles composing the magnetosome chains do not vary with field, since no change in the structure factor (i.e. the SANS signal in the low q -range) is observed. Therefore, we can conclude that within the freeze-dried bacteria the internal microstructure is not altered by external fields, which makes them a good system to characterize the magnetic properties of the individual magnetosome chains.

For the magnetization measurements the bacteria powder was introduced in a gelatin

capsule and investigated with a superconducting quantum interference device magnetometer (Quantum Design MPMS-3) in DC mode. We collected isothermal remanence magnetization (IRM) and direct current demagnetization (DCD) curves, as well as an isothermal magnetization loop at room-temperature. The IRM curve was obtained by measuring the remanence from the initially demagnetized state by taking the sample through successive minor loops from 0 to 1 T. In a similar manner, the DCD curve was obtained by a progressive demagnetization of the initially saturated sample. And the isothermal magnetization loop was measured between 1 and -1 T in continuous mode. Additionally, we measured first-order reversal curves (FORC) with a customized vibrating sample magnetometer between a saturating field of 0.1 T and increasing reversal fields, until reaching finally the major loop. The resulting FORC diagrams were generated from a total of 80 minor loops according to.²⁵

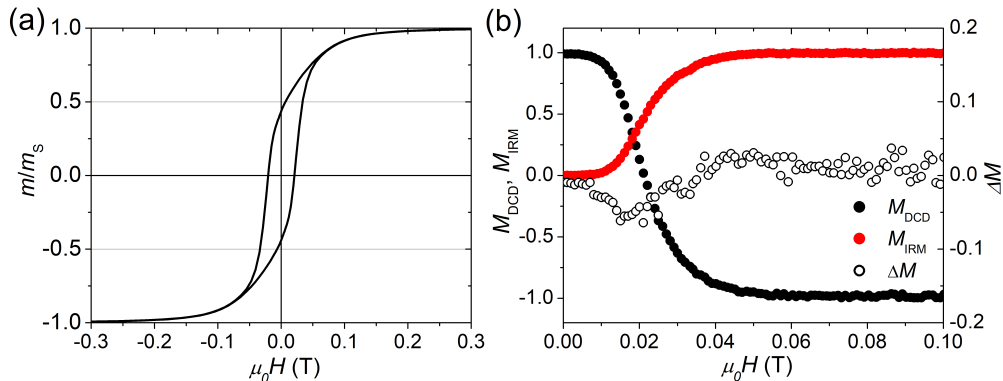


Figure 4: Isothermal, room-temperature magnetization measurements of the freeze-dried bacteria powder: (a) Normalized magnetization curve. (b) Normalized remanence curves M_{DCD} and M_{IRM} , and the modified Henkel plot ΔM (Eq. 2).

Fig. 4(a) displays the isothermal magnetization curve of the powder of the freeze-dried bacteria. This was a loose powder and thus it is safe to assume that the bacteria and hence the 1D chains were randomly oriented (i.e. isotropic ensemble). The curve is fully saturated at around 0.3 T and exhibits a hysteresis with a coercive field of $\mu_0 H_c = 22$ mT and a reduced remanence of $m_r/m_s = 0.45$. This is close to the expected value of 0.5 for an isotropic ensemble of single-domain nanoparticles with uniaxial anisotropy (i.e. Stoner-Wohlfarth particles).²⁴ This indicates that during the magnetization process (i) a mechanical

particle rotation and (ii) dipolar interactions are negligible, because both would reduce the remanence significantly.^{26–28} But to further evaluate the amount of dipolar interactions we performed modified Henkel and FORC measurements.

Fig. 4(b) shows the field-dependence of the normalized isothermal remanence magnetization (IRM) and direct current magnetization (DCD) curves, with $M = m/m_r$. Note that M_{IRM} starts in the demagnetized state ($m/m_r = 0$), and saturates at the maximum remanent magnetization with $m/m_r = 1$, while M_{DCD} starts at 1 and finishes at -1. For the ideal case of non-interacting, uniaxial, single-domain nanoparticles the two remanence curves are related according to the Wohlfarth model ($M_{\text{DCD}}(H) = 1 - 2M_{\text{IRM}}(H)$).²⁴ However, if inter-particle interactions appear the relation between M_{IRM} and M_{DCD} is expected to deviate from the Wohlfarth relation, which can be tested *via* the modified Henkel plot:

$$\Delta M = M_{\text{DCD}} - (1 - 2M_{\text{IRM}}). \quad (2)$$

The sign of ΔM provides information about the nature of the interactions, and traditionally negative values ($\Delta M < 0$) are interpreted as a sign for the presence of dipolar interactions.²⁹ For the magnetosome chains (see Fig. 4(b)), we find that ΔM is slightly negative around $\mu_0 H_c$. However, the deviation is small, at least in comparison to strongly interacting systems.²⁸

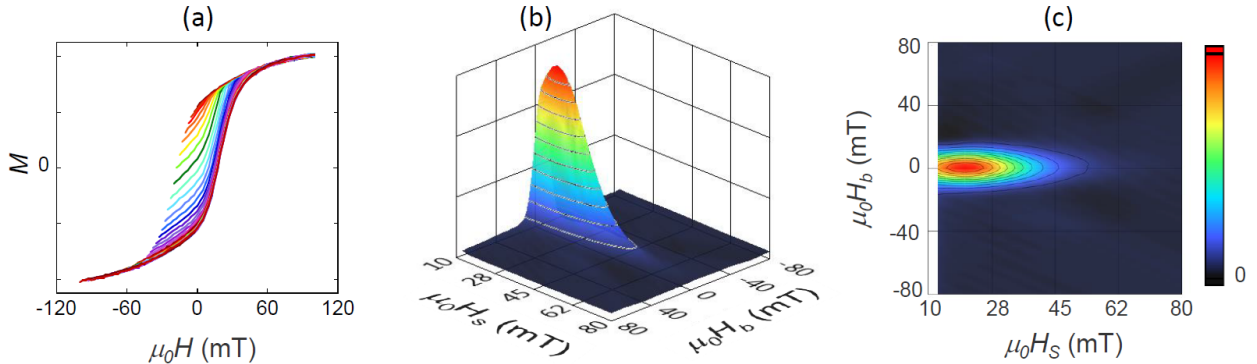


Figure 5: (a) Set of 80 room-temperature FORC measurements in arbitrary units, and (b) the resulting 3D FORC diagram and (c) the contour plot protected in the (H_S, H_B) plane.

A more sensitive approach to evaluate the magnitude of interactions are FORC measure-

ments.^{30,31} In these curves, the magnetization, \vec{M} , is recorded as a function of the applied field, $\mu_0 H$, from the so-called reversal field ($\mu_0 H_R$) up to some positive maximum value (here 100 mT). Then, the complete set of FORCs is obtained by varying the reversal field in discrete steps between the maximum and the minimum field (here -100 mT). Fig. 5(a) shows a group of FORCs (80 curves), measured at room temperature, obtained between 100 and -100 mT in steps of 2.5 mT, that fills the interior of the major hysteresis loop. These measurements give rise to the FORC distribution presented in Figs. 5(b) and (c) (3D representation and contour plot, respectively), which is calculated from the mixed second order derivative of the magnetization²⁵

$$\rho(H_R, H) = -\frac{1}{2} \frac{\partial^2 M}{\partial H_R \partial H} \quad (3)$$

and plotted as a function of the switching field, $H_s = (H - H_R)/2$, and the local interactions field, $H_B = (H + H_R)/2$. The obtained distribution shows an elongated shape which increases rapidly, similar to a step function and decreases exponentially, as expected for randomly oriented, single-domain particles. Moreover, the distribution presents a maximum at around $\mu_0 H_S = 20$ mT, which is consistent with the coercive field of the complete hysteresis loop (see Fig. 4(a)), and the fact that the distribution is highly peaked on the $H_B = 0$ axis is also characteristic of a non-interacting system.

Our magnetometry results are in good agreement with a previous study,³² and we can conclude from them that dipolar interactions between the particles within the 1D chains seem to be in fact negligible and that the magnetic energy of the individual particles is simply dominated by the magnetic (uniaxial) anisotropy. Additionally, the isothermal magnetization curve indicates that in the freeze-dried bacteria the magnetosomes do not mechanically rotate even at high fields (i.e. high magnetic torques), which implies a strong elastic coupling between the magnetosomes and the cellular surrounding.

To summarize, we investigate here the magnetic response of a powder of freeze-dried

M. gryphiswaldense by magnetometry and polarized SANS. The magnetosomes are around 40 nm in size and arranged in linear chains inside the bacteria. We can conclude that the magnetosomes inside the freeze-dried bacteria do not physically rotate in field direction also in presence of large magnetic fields (i.e. large magnetic torques), meaning that an alignment of the particle moments in field-direction occurs exclusively by a Néel-like rotation, and that the particle chains remain intact also after application of large fields of up to 1 T. This is in contrast to studies of colloidal dispersions of such bacteria, where already small magnetic fields of around 30 mT were found to break-up the magnetosome chains,^{16,17} which indicates that the freeze-drying of the bacteria results in mechanically stable configurations of the magnetosome chains. Thus, freeze-dried bacteria can be regarded as model samples to study the magnetization behavior of such 1D magnetosome chains. Here, we can confirm with magnetometry that the quite large magnetosomes in our sample are single-domain particles with uniaxial anisotropy and that dipolar interactions, which play a vital role during the chain formation, have in fact no significant influence on the isothermal magnetization behavior of the magnetosome chains, which verifies that the particles are arranged preferentially with their anisotropy axes along the chain axis.

Acknowledgments

We thank the Science and Technology Facilities Council (STFC) for granting beamtime at the instrument Larmor. P. Bender acknowledges financial support from the National Research Fund of Luxembourg (CORE SANS4NCC grant) and L. Marcano acknowledges the Basque Government for her fellowship (POS_2018_1_0070). This project has received additional funding from the European Commission Framework Programme 7 under grant agreement no 604448 (NanoMag), and the Spanish Government is acknowledged for funding under project number MAT2017-83631-C3-R.

References

1. Bazylinski, D. A.; Frankel, R. B. Magnetosome formation in prokaryotes. *Nat. Rev. Microbiol.* **2004**, *2*, 217–230.
2. Khalil, I. S.; Pichel, M. P.; Abelmann, L.; Misra, S. Closed-loop control of magnetotactic bacteria. *Int. J. Rob. Res.* **2013**, *32*, 637–649.
3. Fdez-Gubieda, M. L.; Muela, A.; Alonso, J.; Garcia-Prieto, A.; Olivi, L.; Fernandez-Pacheco, R.; Barandiaran, J. M. Magnetite Biomineralization in *Magnetospirillum gryphiswaldense*: Time-Resolved Magnetic and Structural Studies. *ACS Nano* **2013**, *7*, 3297–3305.
4. Orue, I.; Marcano, L.; Bender, P.; García-Prieto, A.; Valencia, S.; Mawass, M. A.; Gil-Cartón, D.; Alba Venero, D.; Honecker, D.; García-Arribas, A.; Fernández Barquín, L.; Muela, A.; Fdez-Gubieda, M. L. Configuration of the magnetosome chain: a natural magnetic nanoarchitecture. *Nanoscale* **2018**, *10*, 7407–7419.
5. Yuan, J.; Xu, Y.; Mueller, A. H. One-dimensional magnetic inorganic–organic hybrid nanomaterials. *Chem. Soc. Rev.* **2011**, *40*, 640–655.
6. Wang, H.; Yu, Y.; Sun, Y.; Chen, Q. Magnetic nanochains: a review. *Nano* **2011**, *6*, 1–17.
7. Cēbers, A. Flexible magnetic filaments. *Curr. Opin. Colloid Interface Sci.* **2005**, *10*, 167–175.
8. Dreyfus, R.; Baudry, J.; Roper, M. L.; Fermigier, M.; Stone, H. A.; Bibette, J. Microscopic artificial swimmers. *Nature* **2005**, *437*, 862.
9. Kiani, B.; Faivre, D.; Klumpp, S. Elastic properties of magnetosome chains. *New J. Phys.* **2015**, *17*, 043007.

10. Wolf, H.; Birringer, R. Pattern formation in an array of magnetic nanoscale rods mimics magnetic-dipole interaction-driven spinodal decomposition. *J. Appl. Phys.* **2005**, *98*, 074303.
11. Korth, B. D.; Keng, P.; Shim, I.; Bowles, S. E.; Tang, C.; Kowalewski, T.; Nebesny, K. W.; Pyun, J. Polymer-coated ferromagnetic colloids from well-defined macromolecular surfactants and assembly into nanoparticle chains. *J. Am. Chem. Soc.* **2006**, *128*, 6562–6563.
12. Nakata, K.; Hu, Y.; Uzun, O.; Bakr, O.; Stellacci, F. Chains of superparamagnetic nanoparticles. *Adv. Mater.* **2008**, *20*, 4294–4299.
13. Prozorov, T.; Bazyliniski, D. A.; Mallapragada, S. K.; Prozorov, R. Novel magnetic nanomaterials inspired by magnetotactic bacteria: Topical review. *Mater. Sci. Eng. R Rep.* **2013**, *74*, 133–172.
14. Marcano, L.; Garcia-Prieto, A.; Munoz, D.; Fernandez Barquin, L.; Orue, I.; Alonso, J.; Muela, A.; Fdez-Gubieda, M. Influence of the bacterial growth phase on the magnetic properties of magnetosomes synthesized by *Magnetospirillum gryphiswaldense*. *Biochim. Biophys. Acta, Gen. Subj.* **2017**, *1861*, 1507–1514.
15. Marcano, L.; Muñoz, D.; Martín-Rodríguez, R.; Orue, I. n.; Alonso, J.; García-Prieto, A.; Serrano, A.; Valencia, S.; Abrudan, R.; Fernández Barquín, L.; García-Arribas, A.; Muela, A.; Fdez-Gubieda, M. L. Magnetic Study of co-doped magnetosome chains. *J. Phys. Chem. C* **2018**, *122*, 7541–7550.
16. Körnig, A.; Dong, J.; Bennet, M.; Widdrat, M.; Andert, J.; Müller, F. D.; Schüler, D.; Klumpp, S.; Faivre, D. Probing the mechanical properties of magnetosome chains in living magnetotactic bacteria. *Nano Lett.* **2014**, *14*, 4653–4659.
17. Blondeau, M.; Guyodo, Y.; Guyot, F.; Gatel, C.; Menguy, N.; Chebbi, I.; Haye, B.; Durand-Dubief, M.; Alphandery, E.; Brayner, R.; Coradin, T. Magnetic-field induced

- rotation of magnetosome chains in silicified magnetotactic bacteria. *Sci. Rep.* **2018**, *8*, 7699.
18. Heyen, U.; Schüler, D. Growth and magnetosome formation by microaerophilic *Magnetospirillum* strains in an oxygen-controlled fermentor. *Appl. Microbiol. Biotechnol.* **2003**, *61*, 536–544.
 19. Schneider, C. A.; Rasband, W. S.; Eliceiri, K. W. NIH Image to ImageJ: 25 years of image analysis. *Nat. Methods* **2012**, *9*, 671.
 20. Honecker, D.; Ferdinand, A.; Döbrich, F.; Dewhurst, C. D.; Wiedenmann, A.; Gómez-Polo, C.; Suzuki, K.; Michels, A. Longitudinal polarization analysis in small-angle neutron scattering. *Eur. Phys. J. B* **2010**, *76*, 209–213.
 21. Disch, S.; Wetterskog, E.; Hermann, R. P.; Wiedenmann, A.; Vainio, U.; Salazar-Alvarez, G.; Bergström, L.; Brückel, T. Quantitative spatial magnetization distribution in iron oxide nanocubes and nanospheres by polarized small-angle neutron scattering. *New J. Phys.* **2012**, *14*, 013025.
 22. Bender, P.; Fock, J.; Frandsen, C.; Hansen, M. F.; Balceris, C.; Ludwig, F.; Posth, O.; Wetterskog, E.; Bogart, L. K.; Southern, P.; Szczerba, W.; Zeng, L.; Witte, K.; Grütner, C.; Westphal, F.; Honecker, D.; González-Alonso, D.; Fernández Barquín, L.; Johansson, C. Relating magnetic properties and high hyperthermia performance of iron oxide nanoflowers. *J. Phys. Chem. C* **2018**, *122*, 3068–3077.
 23. Pedersen, J. S. Analysis of small-angle scattering data from colloids and polymer solutions: modeling and least-squares fitting. *Adv. Colloid Interface Sci.* **1997**, *70*, 171 – 210.
 24. Wohlfarth, E. P. Relations between Different Modes of Acquisition of the Remanent Magnetization of Ferromagnetic Particles. *J. Appl. Phys.* **1958**, *29*, 595–596.

25. Roberts, A. P.; Pike, C. R.; Verosub, First-order reversal curve diagrams: A new tool for characterizing the magnetic properties of natural samples. *J. Geophys. Res.* **2000**, *105*, 28461–28475.
26. Bender, P.; Tschöpe, A.; Birringer, R. Determination of the shear modulus of gelatine hydrogels by magnetization measurements using dispersed nickel nanorods as mechanical probes. *J. Magn. Magn. Mater.* **2013**, *346*, 152–160.
27. Bender, P.; Tschöpe, A.; Birringer, R. Magnetization measurements reveal the local shear stiffness of hydrogels probed by ferromagnetic nanorods. *J. Magn. Magn. Mater.* **2014**, *372*, 187–194.
28. Bender, P.; Krämer, F.; Tschöpe, A.; Birringer, R. Influence of dipolar interactions on the angular-dependent coercivity of nickel nanocylinders. *J. Phys. D: Appl. Phys.* **2015**, *48*, 145003.
29. Fearon, M.; Chantrell, R.; Wohlfarth, E. A theoretical study of interaction effects on the remanence curves of particulate dispersions. *J. Magn. Magn. Mater.* **1990**, *86*, 197–206.
30. Mayergoyz, I. Mathematical models of hysteresis. *IEEE Trans. Magn.* **1986**, *22*, 603–608, 02604.
31. Pike, C. R.; Roberts, A. P.; Verosub, K. L. Characterizing interactions in fine magnetic particle systems using first order reversal curves. *J. Appl. Phys.* **1999**, *85*, 6660–6667.
32. Fischer, H.; Mastrogiacomo, G.; Löffler, J. F.; Warthmann, R. J.; Weidler, P. G.; Gehring, A. U. Ferromagnetic resonance and magnetic characteristics of intact magnetosome chains in *Magnetospirillum gryphiswaldense*. *Earth Planet. Sci. Lett.* **2008**, *270*, 200–208.

Graphical TOC Entry

